

Fragment-based Treatment of Delocalization and Static Correlation Errors in Density-Functional Theory

Jonathan Nafziger

*Department of Chemistry, Purdue University, 560 Oval Dr.,
West Lafayette IN 47907, USA*

Adam Wasserman^{a)}

*Department of Chemistry, Purdue University, 560 Oval Dr.,
West Lafayette IN 47907, USA and*

*Department of Physics and Astronomy, Purdue University, 525 Northwestern Ave.,
West Lafayette, IN 47907, USA*

One of the most important open challenges in modern Kohn-Sham (KS) density-functional theory (DFT) is the correct treatment of systems involving fractional electron charges and spins. Approximate exchange-correlation (XC) functionals struggle with such systems, leading to pervasive delocalization and static correlation errors. We demonstrate how these errors, which plague density-functional calculations of bond-stretching processes, can be avoided by employing the alternative framework of partition density-functional theory (PDFT) even with simple local and semi-local functionals for the fragments. Our method is illustrated with explicit calculations on simple systems exhibiting delocalization and static-correlation errors, stretched H_2^+ , H_2 , He_2^+ , Li_2^+ , and Li_2 . In all these cases, our method leads to greatly improved dissociation-energy curves. The effective KS potential corresponding to our self-consistent solutions display key features around the bond midpoint; these are known to be present in the exact KS potential, but are absent from most approximate KS potentials and are essential for the correct description of electron dynamics.

^{a)}Corresponding Author: awasser@purdue.edu

1. INTRODUCTION

Fifty years after its proposal, the Kohn-Sham (KS) prescription¹ of density-functional theory (DFT)² continues to be one of the most practical formulations of the many-electron problem in quantum chemistry and solid-state physics. Improving on the accuracy and efficiency of KS-DFT calculations is a constant and pressing goal for the electronic-structure community³, which works on understanding the sources of errors⁴⁻⁷, developing new exchange-correlation (XC) functionals⁸⁻¹⁰, and designing better and faster computational algorithms¹¹.

Two open problems in DFT are the delocalization and static correlation errors of approximate functionals, arising from improper treatment of fractional charges and spins, respectively⁴⁻⁷. Delocalization errors cause underestimation of energies in dissociating molecular ions, chemical reaction barrier heights, charge-transfer excitations, band-gaps of semiconductors, as well as overestimation of binding energies of charge-transfer complexes and response to electric fields. Static correlation errors are responsible for the problems with degenerate and near-degenerate states, incorrect dissociation limit of neutral diatomics and poor treatment of strongly correlated systems. The simplest systems that display these errors are stretched H_2^+ , H_2 , He_2^+ , Li_2^+ , and Li_2 . Local and semi-local approximations to the exchange-correlation energy (E_{xc}) severely underestimate the dissociation energy of H_2^+ , He_2^+ and Li_2^+ due to delocalization, and overestimate the dissociation energy of H_2 and Li_2 due to static correlation (See Figure 1).

In this work we demonstrate that partition density-functional theory (PDFT)¹² is a suitable framework to solve these problems. The *partition energy* of PDFT (denoted E_p , to be defined below) is amenable to simple approximations which can handle delocalized and statically-correlated electrons, greatly improving dissociation curves. For example, Fig. 1 displays the results we obtained by applying PDFT with the Local Density Approximation (LDA) and a simple “Overlap Approximation” (OA) for E_p (defined in Eq.5) as compared to standard KS-LDA results. We are not aware of approximate XC-functionals that yield similar accuracy for all these systems within standard KS-DFT.

PDFT allows a molecular calculation to be performed on individual fragments of a molecule rather than on the molecule as a whole. It is based on the density-partitioning scheme of refs. [13] and [14], and is nearly equivalent in practice to the formulation of em-

bedding theory by Huang and Carter¹⁵ based on earlier work of Cortona¹⁶ and Wesolowski and Warshel¹⁷ (see refs. [18] and [19] for recent reviews on subsystem-DFT). One critical difference, essential for this work, is our use of *ensemble* functionals to treat non-integer electron numbers and spins in fragments of molecules. Kraisler and Kronik have also recently used ensemble-generalized functionals to solve issues with fractional charges in dissociation problems²⁰, but PDFT allows the use of these functionals at finite separations rather than being limited to completely isolated fragments.

2. PDFT

A detailed overview of PDFT may be found in ref. [22]. Here we only provide a brief summary. The first step of PDFT is to partition the molecule into fragments. This is done by dividing the nuclear potential into fragment potentials, $v_\alpha(\mathbf{r})$. This is the only choice the PDFT user makes in regards to the fragmentation and after this choice the fragment densities are uniquely determined¹³. We typically choose atom-based fragments, where each nucleus controls its own fragment, but any partition may be chosen as long as the sum of fragment potentials equals the total external nuclear potential.

Each individual fragment calculation is a standard DFT calculation for each of the ensemble components of the ground-state density of N_α electrons in an effective potential. We denote the i^{th} component of the α^{th} fragment spin σ density as $n_{i\alpha\sigma}(\mathbf{r})$. The number of electrons in each fragment's ensemble spin component, $N_{i\alpha\sigma} = \int n_{i\alpha\sigma}(\mathbf{r})d\mathbf{r}$, will always be an integer number of electrons, but the total number of electrons of a given spin in a given fragment,

$$N_{\alpha\sigma} = \sum_i f_{i\alpha} N_{i\alpha\sigma} \tag{1}$$

will not necessarily be an integer. Here, the $f_{i\alpha}$ are the ensemble coefficients, which satisfy the sum rule, $\sum_i f_{i\alpha} = 1$. The energy of these fragments is given by,

$$E_\alpha = \sum_i f_{i\alpha} E_\alpha[n_{i\alpha\uparrow}, n_{i\alpha\downarrow}] \tag{2}$$

Here, the subscript α on the energy denotes that this is the energy corresponding to the $\{n_{i\alpha\sigma}\}$ in the external potential $v_\alpha(\mathbf{r})$ rather than the total external potential. The effective *external* potential for each fragment is the sum of the fragment's potential, $v_\alpha(\mathbf{r})$, and the

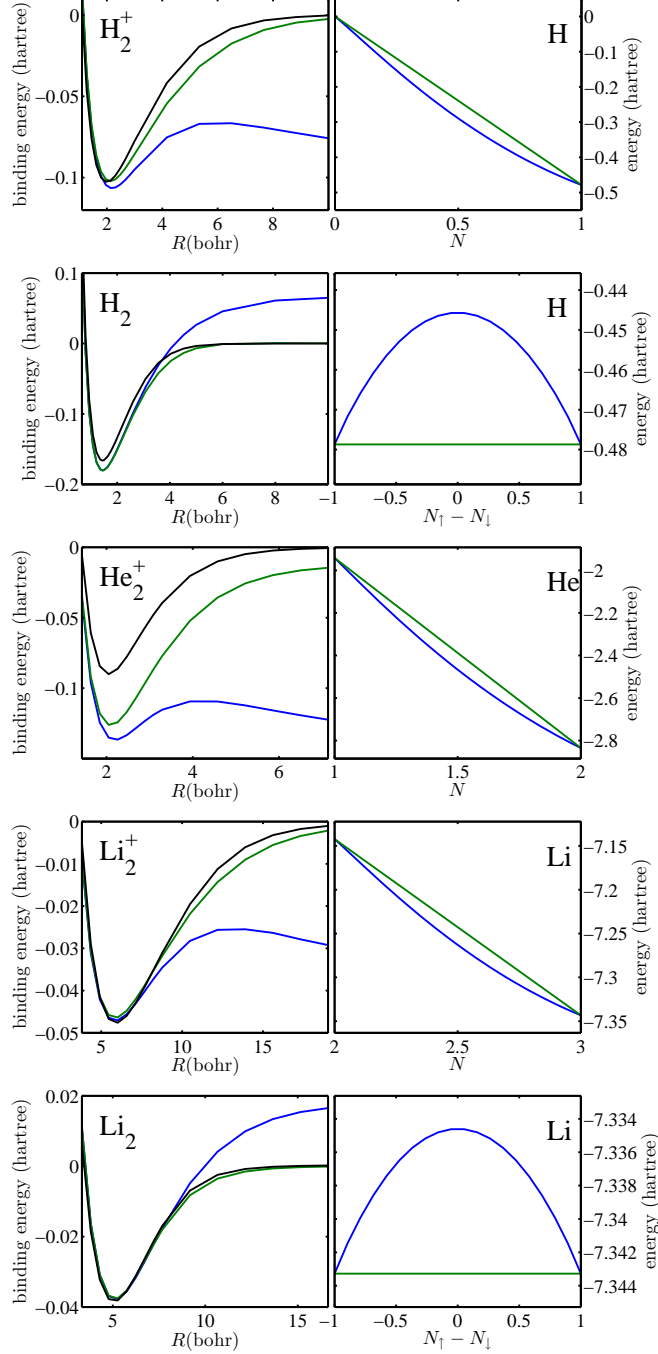


FIG. 1. Left column: Dissociation curves for five dimers. In blue are the KS-LDA results, in green are the OA-LDA PDFT results and in black are CCSD/aug-cc-pVDZ calculations performed in NWChem²¹ (except for H_2^+ , which is simply a one-electron non-interacting calculations). Right column: Energies of monomers for fractional charges and spins. In blue are the KS-LDA energies evaluated for these fractional charges and spins and the green curves are the PDFT fragment energies. The maximum difference between the blue and green curves in the right column account for half the difference between the blue and green curves in the dissociation limit (Left column).

partition potential, $v_{p\sigma}(\mathbf{r})$. The latter is a *global* quantity ensuring that the fragment calculations produce densities that sum to yield the correct molecular density while minimizing the sum of the fragment energies, E_f . The partition potential enters formally as a lagrange multiplier constraining the fragment densities to equal the molecular density, but can be calculated as the functional derivative of E_p with respect to the total density²³.

The partition energy, E_p , central to our work, is the difference between the total molecular energy, $E[n]$, and the sum of the fragment energies, $E_f = \sum_{\alpha} E_{\alpha}$. As argued in ref. [23], the minimum value of E_f with respect to variations of the $n_{i\alpha\sigma}$'s is a functional of the total density. Subtracting this quantity from the true ground-state energy yields $E_p[n] = E[n] - E_f[n]$, an implicit functional of the molecular density. We may also write E_p as an explicit functional of the fragment densities: $E_p[\{n_{i\alpha\sigma}\}] = E[n_f] - E_f[\{n_{i\alpha\sigma}\}]$. In the two-fragment case where each fragment has two ensemble components, E_p can be divided into components and written out explicitly in terms of fragment densities:

$$E_p[\{n_{i\alpha\sigma}\}] = T_s^{\text{nad}}[\{n_{i\alpha\sigma}\}] + V_{\text{ext}}^{\text{nad}}[\{n_{i\alpha\sigma}\}] + E_{\text{H}}^{\text{nad}}[\{n_{i\alpha\sigma}\}] + E_{\text{XC}}^{\text{nad}}[\{n_{i\alpha\sigma}\}] \quad , \quad (3)$$

where each non-additive functional is,

$$F^{\text{nad}}[\{n_{i\alpha\sigma}\}] \equiv F[n_{f\uparrow}, n_{f\downarrow}] - \sum_{i,\alpha} f_{i\alpha} F_{\alpha}[n_{i\alpha\uparrow}, n_{i\alpha\downarrow}]. \quad (4)$$

These are similar to the non-additive functionals of embedding theory¹⁵⁻¹⁷ except that the functional values for each fragment are calculated from ensembles, rather than being evaluated on total fragment densities. In practice, a choice of density-functional approximation (DFA) must be made for E_{XC} and $E_{\text{XC}}^{\text{nad}}$. In addition, T_s^{nad} requires writing the non-interacting kinetic energy as a functional of the density. Approximate kinetic energy functionals may be used²⁴, although T_s^{nad} can also be obtained from an inversion of the sum of fragment densities as in ref. [25]. We use a similar inversion method for He_2^+ , Li_2^+ and Li_2 , and we use von Weizsäcker inversion for H_2^+ and H_2 , since these systems have a single occupied orbital.

For a given choice of XC functional, we may *exactly* reproduce the corresponding KS-DFT calculation as long as the same DFA is employed for both $E_{\text{XC}}^{\text{nad}}$ and E_f ²⁶. We can also trivially reproduce a KS-DFT calculation by setting the number of fragments equal to one. In these ways PDFFT subsumes KS-DFT.

3. APPROXIMATING THE PARTITION ENERGY FUNCTIONAL

However, PDFT also goes beyond KS-DFT. For example, the following ‘‘Overlap Approximation’’ to the partition energy functional produces the results displayed in Fig. 1 when used with LDA:

$$E_p^{\text{OA}} = T_s^{\text{nad}} + V_{\text{ext}}^{\text{nad}} + E_{\text{H}}^{\text{nad}} + S E_{\text{xc}}^{\text{nad}} + (1 - S) \Delta E_{\text{H}}^{\text{nad}} , \quad (5)$$

where $\Delta E_{\text{H}}^{\text{nad}}$ is a correction to the non-additive hartree (to be discussed after its definition in Eq. 10) , valid at larger separations, and S is a functional of the fragment densities defined by:

$$S[n_A, n_B] = \text{erf}\left(C \int \sqrt{n_A(\mathbf{r})n_B(\mathbf{r})} d\mathbf{r}\right) . \quad (6)$$

The densities, $n_A(\mathbf{r})$ and $n_B(\mathbf{r})$ refer to fragment densities summed over the ensemble and spin components. The overlap measure, S , is designed to go to zero at infinite fragment separation and to one at equilibrium distances (reminiscent of the work of ref. [27]). When $S = 1$ the partition energy matches eq. 3, and thus the total energy will simply reproduce the standard KS energy for a given choice of XC functional. As $S \rightarrow 0$, the non-additive XC energy is turned off and a correction to the non-additive hartree, $\Delta E_{\text{H}}^{\text{nad}}$, is turned on. There is one parameter C , which we have set to $C = 2$ to yield the results in Fig. 1. The values of the overlap measure, S , from these calculations are plotted in Fig. 2.

Clearly, the separation of E_p and E_f opens opportunities for new approximations within a self-consistent framework. In particular, when the error of a DFT calculation is due to fragmentation, as in bond-stretching, expressing E_p as a functional of the set of fragment densities has the potential of fixing the error from its root. The physics of *inter*-fragment interactions is contained in E_p while that of *intra*-fragment interactions is contained in E_f . This is the main idea we wish to explore in the remainder of this paper. We first discuss a consequence of using different levels of approximation for E_p and E_f . As shown in ref. [23], the partition potential is determined from the chain rule (spin notation is suppressed here and below for simplicity):

$$v_p(\mathbf{r}) = \sum_{\alpha} \int d\mathbf{r}' v_{p,i\alpha}(\mathbf{r}') Q_{i\alpha}(\mathbf{r}', \mathbf{r}) , \quad (7)$$

where the $\{i, \alpha\}^{\text{th}}$ component of the partition potential is given by

$$v_{p,i\alpha}(\mathbf{r}) = \frac{\delta E_p}{\delta n_{i\alpha}(\mathbf{r})} \quad (8)$$

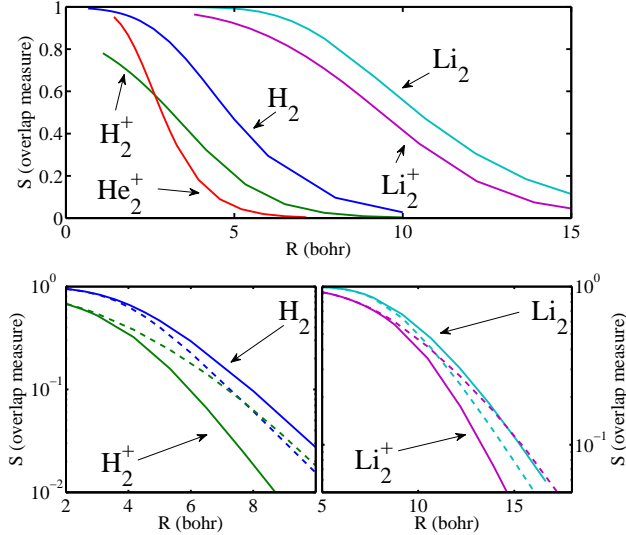


FIG. 2. Overlap measure of Eq. 6 for various separations. Top: Overlap measure calculated on self consistent densities from standard PDF-T calculations (using Eq. 3) which do not depend directly on the overlap measure. The bottom two (logarithmic) plots compare the overlap measure evaluated for densities from PDF-T calculations using Eq. 3 (solid) and the OA, Eq. 5, (dashed). We see that when the OA is employed, the overlap measure is increased in the cases of H_2^+ and Li_2^+ , while in the cases of H_2 and Li_2 the overlap measure is reduced.

and $Q_{i\alpha}(\mathbf{r}', \mathbf{r}) = \delta n_{i\alpha}(\mathbf{r}') / \delta n(\mathbf{r})$ satisfies the sum-rule: $\sum_{i,\alpha} Q_{i\alpha}(\mathbf{r}', \mathbf{r}) = \delta(\mathbf{r}' - \mathbf{r})$. As long as the same level of approximation is employed for E_p and E_f , then at convergence $v_{p,i\alpha}(\mathbf{r}) = v_{p,j\beta}(\mathbf{r}) \forall \alpha, \beta, i, j$, so the choice of $Q_{i\alpha}$ is inconsequential provided the sum-rule is satisfied. When different levels of approximation are used for E_p and E_f , however, the $v_{p,\alpha}(\mathbf{r})$ are not necessarily identical at convergence, and it becomes critical to specify the approximation being used for the $Q_{i\alpha}$. Future work will need to establish the effect of different approximations for Q on final energies and densities. Throughout the present work, we employ the Local-Q approximation suggested in ref. [23]:

$$Q_{i\alpha}(\mathbf{r}, \mathbf{r}') = \delta(\mathbf{r} - \mathbf{r}') \frac{n_{i\alpha}(\mathbf{r})}{n_f(\mathbf{r}')} \quad (9)$$

We now have all of the necessary tools to perform PDF-T calculations with separate approximations for E_f and E_p . We implemented PDF-T on a real-space prolate spheroidal grid, following the work of Becke and other workers²⁸⁻³², and found XC potentials and energies through use of the Libxc library³³. We validated the code through calculations on H_2^+ , H_2 , and Li_2 at equilibrium geometries where our code yields the same energies to within

10^{-7} hartrees for for both PDFT (Using Eq. 3) and standard KS-DFT calculations. (see table I for a sample of such comparisons). NWChem was used for reference CCSD/aug-cc-pVDZ calculations²¹. We now look at the delocalization and static-correlation errors from the point of view of PDFT, and demonstrate our proposed solutions.

Li ₂ LDA @ R = 5.120 bohr		H ₂ LDA @ R = 1.446 bohr		H ₂ ⁺ Exact @ R = 2.0 bohr	
KS-DFT ³²	PDFT	KS-DFT ³²	PDFT	KS-DFT ²⁹	PDFT
14.7245	-14.724457	-1.137692	-1.1376923	-0.6026342144(7)	-0.60263425

TABLE I. Comparison of total energies in hartree, for our PDFT code, and from benchmark KS-DFT calculations.

4. DELOCALIZATION

We first consider the accuracy of E_p vs. E_f in H_2^+ , He_2^+ and Li_2^+ . Since the Hamiltonian in these cases has inversion symmetry, and the total number of electrons in each case is odd, the correct ground-state density has fractional numbers of electrons on the left and right sides. In the case of H_2^+ this means “half an electron” on the left and “half an electron” on the right, but the correct ground-state energy at infinite separation is that of an isolated hydrogen atom (-0.5 hartree). A correct size-consistent electronic-structure method must therefore assign an energy of -0.25 hartree to a hydrogen atom with *half* an electron. This same argument may be extended to dissociating hydrogen chains, resulting in the conclusion that the energy is a piecewise-linear function of electron number³⁴. In the other two cases (He_2^+ and Li_2^+) this indicates that the correct energy of a fragment at infinite separation is a linear interpolation between two electronic systems with integer number of electrons: one with one more electron than the other. This is of course accomplished by the exact grand-canonical ensemble functional³⁵, but it is *not* accomplished by most approximate functionals, as can be seen in Fig.1 for LDA^{36,37}. For H_2^+ the self-interaction error $SIE = E_H[n] + E_{xc}[n]$ is a convex function of electron number N . As a consequence, LDA underestimates the energy for half an electron in a hydrogen atom. Two times this error is precisely $E_H(\infty)^{nad} + E_{xc}(\infty)^{nad}$ in Eq.(3), the LDA delocalization error of H_2^+ at infinite separation. The OA of Eq.5 works by suppressing this error as $S(\infty) = 0$ and reproduces the LDA at the equilibrium separation.

Because PDFT treats each fragment using an ensemble, the fragment calculation for the left or right half of stretched H_2^+ is a linear interpolation between open shell calculations for zero and one electron. For He_2^+ the two ensemble components contain 1 and 2 electrons, i.e. for fragment A : $N_{1A} = 1$, $N_{2A} = 2$, $f_{1A} = 1/2$ and $f_{2A} = 1/2$. For Li_2^+ the ensemble components contain 2 and 3 electrons ($N_{1A} = 2$, $N_{2A} = 3$, $f_{1A} = 1/2$ and $f_{2A} = 1/2$). The energies and densities are linear interpolations between these ensemble components. We call this interpolation ensemble-LDA (ELDA), and plot the resulting curves in the right hand column of Fig. 1. Even LDA provides reasonable approximations for E_f because each fragment calculation is done for a well-localized density with an integer number of electrons. The ensemble formulation then provides the correct scaling for the energy of each fragment with respect to number of electrons in that fragment. Thus, overall, our conclusion is that E_f is reasonably accurate and it is E_p which is causing error in the dissociation limit. We now explain how Eq. 5 corrects E_p .

While in the case of H_2^+ it is clear that $E_{\text{H}}(\infty)^{\text{nad}}$ is entirely equal to the self-interaction error, the cases of He_2^+ and Li_2^+ must be treated with more care. This is the reason for the $\Delta E_{\text{H}}^{\text{nad}}$ term in Eq. 5. This correction is defined as

$$\Delta E_{\text{H}}^{\text{nad}} \equiv \frac{1}{4} \sum_{\alpha \neq \beta} \sum_{i,j} g_{i,j} f_{i\alpha} \int \frac{n_{iA}(\mathbf{r}) n_{jB}(\mathbf{r}')}{|\mathbf{r} - \mathbf{r}'|} d\mathbf{r} d\mathbf{r}' - E_{\text{H}}^{\text{nad}}, \quad (10)$$

where $g_{i,j} = 0$ if $N_{i\alpha} + N_{j\beta} \neq N$ and $g_{i,j} = 1$ if $N_{i\alpha} + N_{j\beta} = N$. This makes it so that the ensemble component with one less electron on one fragment will only interact with the ensemble component with one more electron on the other fragment and vice-versa. In the case of H_2^+ this means that the correction term is simply $-E_{\text{H}}^{\text{nad}}$ because the lower ensemble component has no electrons. In the case of Li_2^+ , for each fragment, one ensemble component has two electrons and the other has three electrons. The first term of this interaction will simply be a fifty percent mixture of the electrostatic interaction between the two-electron component density on one fragment with the three-electron component density on the other side and vice-versa. For cases where the ensemble components have the same total number of electrons such as H_2 and Li_2 , the first term is exactly equal to $E_{\text{H}}^{\text{nad}}$ and this correction has no effect.

This approximation was inspired in part by range-separated hybrid (RSH) functionals³⁸. In RSH functionals, a larger portion of exact exchange is included in long-range interactions to improve accuracy. The distinction between long-range and short-range is made by a

tunable parameter. In our case we also attempt to use an improved approximation for the long-range interaction, but our distinction between long and short range is contained in the separation of E_f and E_p .

5. STATIC-CORRELATION

We next see how this idea can be applied successfully to handle static correlation, taking H_2 as an example. As in the H_2^+ case, we first consider the dissociation products of H_2 : two isolated hydrogen atoms, with a total energy of -1.0 hartree. However, the molecular calculation is spin-neutral, and it remains spin-neutral throughout dissociation due to inversion symmetry. Therefore, each dissociating hydrogen atom has an electron which is “half spin up” and “half spin down”. The exact functional assigns an energy to this fragment equal to that of a spin-up electron in a hydrogen atom. This is known as the constancy condition⁷. However, approximate functionals do not show this behaviour and typically overestimate the energy of a system with fractional spins. This overestimation exactly matches the static correlation error of dissociated H_2 , and is given by $E_{xc}^{nad}(\infty)$. Once again, Eq.5 works by suppressing this error as $S(\infty) = 0$.

Each fragment in an H_2 PDFT calculation contains one electron, but the energies and spin-densities are considered to be ensembles of a spin-up and a spin-down electron, i.e. $N_{1A\uparrow} = 1$, $N_{1A\downarrow} = 0$, $N_{2A\uparrow} = 0$, $N_{2A\downarrow} = 1$, $f_{1A} = 1/2$ and $f_{2A} = 1/2$. The energies and densities are then linear interpolations between a spin-up ensemble component and a spin-down ensemble component. The case of Li_2 is similar. The dissociation products are two isolated Li atoms. The ensembles in a Li fragment within PDFT consist of two components: one with two spin-up electrons and one spin-down electron and the other with one spin-up electron and two spin-down electrons ($N_{1A\uparrow} = 1$, $N_{1A\downarrow} = 2$, $N_{2A\uparrow} = 2$, $N_{2A\downarrow} = 1$). These two cases are degenerate so the fragment energies satisfy the constancy condition. The energies and densities of these fragments are linear interpolations between these ensemble components. As in the H_2 case, E_f is accurate with standard DFA’s and we only need to improve E_p .

The OA of Eq. 5 works by imposing size-consistency on the partition energy: at infinite separation E_p must vanish. For H_2 and Li_2 the only part of E_p which does not go to zero is the E_{xc}^{nad} term. Thus, the OA suppresses it through multiplication by S .

6. PEAK IN THE KS POTENTIAL

It is well known that the KS potential for stretched H_2 develops a peak at the bond midplane^{39–45}. This exact feature of $v_s(\mathbf{r})$, is essential for the correct description of dissociation and electron dynamics within KS-DFT^{46,47}. While certain sophisticated XC functionals such as those based on the random phase approximation can reproduce the peak⁴⁸, it is absent from most approximate DFA’s. It is clear from Fig. 1 that the OA has greatly improved the dissociation energy for H_2 , but we may also explore whether the OA can reproduce this peak in the XC potential. We can derive the molecular XC potential corresponding to a PDFT calculation through the functional derivative of the XC energy, which in the case of PDFT can be broken into fragment pieces and non-additive pieces.

$$\begin{aligned}
 v_{xc,\sigma}(\mathbf{r}) &= \frac{\delta E_{xc}[n_\uparrow, n_\downarrow]}{\delta n_\sigma(\mathbf{r})} \\
 &= \frac{\delta E_f^{XC}[n_\uparrow, n_\downarrow]}{\delta n_\sigma(\mathbf{r})} + \frac{\delta E_p^{XC}[n_\uparrow, n_\downarrow]}{\delta n_\sigma(\mathbf{r})}
 \end{aligned}
 \tag{11}$$

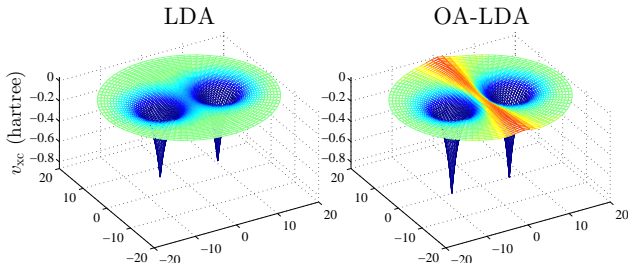


FIG. 3. Effective XC-potentials for two PDFT H_2 calculations with $R = 14$ bohr. The plots show an entire 2D plane along the bonding axis. Nuclei are at $+7$ and -7 on the bond axis. Vertical scale for potentials is in units of hartree and horizontal scale is in bohr.

Fig.3 compares this effective XC potential from two PDFT calculations on stretched H_2 (internuclear separation of 14 bohrs). For the first we use the LDA in both E_f and E_p . For the second we use LDA in E_f and OA-LDA for E_{XC}^{nad} in E_p . We clearly see that the potential corresponding to the OA-LDA calculation has a peak in the bonding midplane. Furthermore, we see that the peak comes entirely from the second term. The two terms of Eq. 11 are plotted separately in Fig. 4.

Helbig, Tokatly and Rubio (HTR) derived an exact form for $v_s(\mathbf{r})$ for any two dissociated

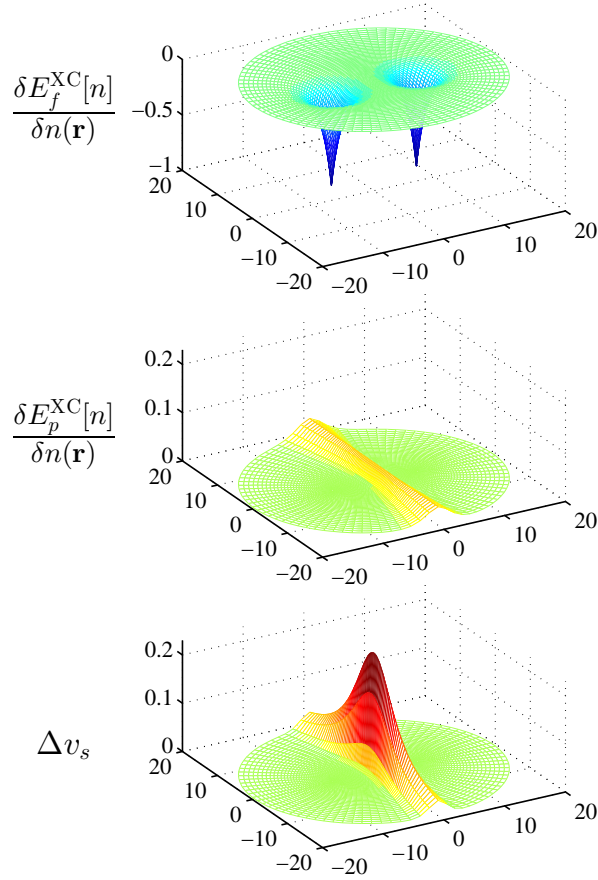


FIG. 4. Top and Middle: Components of the effective XC-potentials for OA-LDA H₂ calculations with R = 14 bohr, corresponding to the first and second terms of Eq. 11. Bottom: Peak in the KS potential from Eq. 12⁴⁴. Nuclei are at +7 and -7 bohr on the bond axis. Vertical scale for potentials is in units of hartree and horizontal scale is in bohr.

particles around the bonding midplane (Eq. 29 in their paper):

$$\Delta v_s(\mathbf{r}) = \frac{[\sqrt{n_A}\nabla\sqrt{n_B} - \sqrt{n_B}\nabla\sqrt{n_A}]^2}{2(n_A + n_B)^2} + \frac{I_A n_A + I_B n_B}{n_A + n_B} - I, \quad (12)$$

where, n_A and n_B are the dissociated atomic densities and I_A, I_B and I are the ionization potentials for the two fragments and the total system respectively. In the case of homonuclear diatomics such as H₂, the second and third terms cancel leaving only the first term which produces a peak determined by the asymptotic behavior of n_A and n_B . HTR derived this expression using the fact that, at dissociation, the exact molecular density is exactly $n_m =$

$n_A + n_B$, and neither the total nor fragment densities are represented by more than one orbital so the von Weizsäcker kinetic energy is exact. In PDFT, the fragment densities n_A and n_B always sum to give the molecular density, so this expression may be evaluated at any finite separation. In fact, Eq. 12 can be identified as $-\delta T_s^{\text{nad}}/\delta n(\mathbf{r})$ from PDFT.

When we compare the peak produced by Eq. 12 to the peak produced by the OA-LDA we see that its shape and size do not quite match. The maximum value from the HTR expression is around 0.24 hartree, while the maximum from the OA-LDA peak is 0.04 hartree. The HTR peak has its maximum at the bond axis and decreases farther away from the bond axis while the OA-LDA peak is flat. Nevertheless, the OA-LDA peak is in the correct location and is localized to the same region in the bonding midplane. Furthermore the fact that the HTR expression exactly matches $-\delta T_s^{\text{nad}}/\delta n(\mathbf{r})$ may help guide further development of functional forms for the OA.

7. CONCLUDING REMARK

The techniques described thus far are specific to homonuclear diatomics, but work is ongoing to extend these ideas to more general systems, including heteronuclear and multifragment systems. Our results suggest that local and semi-local density-functional approximations already do well for the localized fragments involved in the calculation of E_f and attention needs to be placed on developing general approximations for E_p . This paper indicates that the path is worth taking, as even a simple approximation for E_p can achieve via fragment calculations what sophisticated XC-functionals cannot via standard molecular calculations.

Acknowledgments: We acknowledge valuable discussions with Martín Mosquera and Daniel Jensen. This work was supported by the Office of Basic Energy Sciences, U.S. Department of Energy, under grant No.DE-FG02-10ER16196. A.W. also acknowledges support from the Alfred P. Sloan Foundation and the Camille Dreyfus Teacher-Scholar Awards Programs.

REFERENCES

- ¹W. Kohn and L. J. Sham, Phys. Rev. **140**, A1133 (1965).
- ²P. Hohenberg and W. Kohn, Phys. Rev. **136**, B864 (1964).

- ³R. M. Martin, *Electronic structure: basic theory and practical methods* (Cambridge UP, 2004).
- ⁴A. J. Cohen, P. Mori-Sánchez, and W. Yang, *Science* **321**, 792 (2008).
- ⁵P. Mori-Sánchez, A. J. Cohen, and W. Yang, *Phys. Rev. Lett.* **100**, 146401 (2008).
- ⁶P. Mori-Sánchez, A. J. Cohen, and W. Yang, *Phys. Rev. Lett.* **102**, 066403 (2009).
- ⁷A. J. Cohen, P. Mori-Sánchez, and W. Yang, *J. Chem. Phys.* **129**, 121104 (2008).
- ⁸J. P. Perdew, K. Burke, and M. Ernzerhof, *Phys. Rev. Lett.* **77**, 3865 (1996).
- ⁹J. Tao, J. P. Perdew, V. N. Staroverov, and G. E. Scuseria, *Phys. Rev. Lett.* **91**, 146401 (2003).
- ¹⁰Y. Zhao and D. G. Truhlar, *Theor. Chem. Acc.* **120**, 215 (2008).
- ¹¹X. Andrade, J. Alberdi-Rodriguez, D. A. Strubbe, M. J. T. Oliveira, F. Nogueira, A. Castro, J. Muguerza, A. Arruabarrena, S. G. Louie, A. Aspuru-Guzik, A. Rubio, and M. A. L. Marques, *J. Phys.: Condens. Matter* **24**, 233202 (2012).
- ¹²P. Elliott, K. Burke, M. H. Cohen, and A. Wasserman, *Phys. Rev. A* **82**, 024501 (2010).
- ¹³M. H. Cohen and A. Wasserman, *J. Stat. Phys.* **125**, 1121 (2006).
- ¹⁴M. H. Cohen and A. Wasserman, *J. Phys. Chem. A* **111**, 2229 (2007).
- ¹⁵C. Huang and E. A. Carter, *J. Chem. Phys.* **135**, 194104 (2011).
- ¹⁶P. Cortona, *Phys. Rev. B* **44**, 8454 (1991).
- ¹⁷T. A. Wesolowski and A. Warshel, *J. Phys. Chem.* **97**, 8050 (1993).
- ¹⁸C. R. Jacob and J. Neugebauer, *Wiley Interdisciplinary Reviews: Computational Molecular Science* **4**, 325 (2014).
- ¹⁹A. Krishtal, D. Sinha, A. Genova, and M. Pavanello, *Journal of Physics: Condensed Matter* **27**, 183202 (2015).
- ²⁰E. Kraisler and L. Kronik, *Physical Review A* **91**, 032504 (2015).
- ²¹M. Valiev, E. J. Bylaska, N. Govind, K. Kowalski, T. P. Straatsma, H. J. Van Dam, D. Wang, J. Nieplocha, E. Apra, T. L. Windus, *et al.*, *Computer Physics Communications* **181**, 1477 (2010).
- ²²J. Nafziger and A. Wasserman, *The Journal of Physical Chemistry A* **118**, 7623 (2014).
- ²³M. A. Mosquera and A. Wasserman, *Mol. Phys.* **111**, 505 (2013).
- ²⁴T. A. Wesolowski, Y. Ellinger, and J. Weber, *J. Chem. Phys.* **108**, 6078 (1998).
- ²⁵J. D. Goodpaster, N. Ananth, F. R. Manby, and T. F. Miller III, *J. Chem. Phys.* **133**, 084103 (2010).

- ²⁶J. Nafziger, Q. Wu, and A. Wasserman, *J. Chem. Phys.* **135**, 234101 (2011).
- ²⁷J. Morales and T. J. Martínez, *J. Phys. Chem. A* **108**, 3076 (2004).
- ²⁸A. D. Becke, *J. Chem. Phys.* **76**, 6037 (1982).
- ²⁹A. Makmal, S. Kümmel, and L. Kronik, *J. Chem. Theory Comput.* **5**, 1731 (2009).
- ³⁰J. Kobus, L. Laaksonen, and D. Sundholm, *Comput. Phys. Commun.* **98**, 346 (1996).
- ³¹L. Laaksonen, P. Pyykkö, and D. Sundholm, *Int. J. Quant. Chem.* **23**, 309 (1983).
- ³²T. Grabo, T. Kreibich, and E. K. U. Gross, *Mol. Eng* **7**, 27 (1997).
- ³³M. A. Marques, M. J. Oliveira, and T. Burnus, *Comput. Phys. Commun.* **183**, 2272 (2012).
- ³⁴W. Yang, Y. Zhang, and P. W. Ayers, *Phys. Rev. Lett.* **84**, 5172 (2000).
- ³⁵J. P. Perdew, R. G. Parr, M. Levy, and J. L. Balduz Jr, *Phys. Rev. Lett.* **49**, 1691 (1982).
- ³⁶P. A. M. Dirac, *Math. Proc. Cambridge* **26**, 376 (1930).
- ³⁷J. P. Perdew and Y. Wang, *Phys. Rev. B* **45**, 13244 (1992).
- ³⁸R. Baer, E. Livshits, and U. Salzner, *Annu. Rev. Phys. Chem.* **61**, 85 (2010).
- ³⁹M. A. Buijse, E. J. Baerends, and J. G. Snijders, *Phys. Rev. A* **40**, 4190 (1989).
- ⁴⁰R. van Leeuwen and E. J. Baerends, *Phys. Rev. A* **49**, 2421 (1994).
- ⁴¹O. V. Gritsenko, R. van Leeuwen, and E. J. Baerends, *Phys. Rev. A* **52**, 1870 (1995).
- ⁴²O. V. Gritsenko and E. J. Baerends, *Phys. Rev. A* **54**, 1957 (1996).
- ⁴³O. V. Gritsenko and E. J. Baerends, *Theor. Chem. Acc.* **96**, 44 (1997).
- ⁴⁴N. Helbig, I. V. Tokatly, and A. Rubio, *J. Chem. Phys.* **131**, 224105 (2009).
- ⁴⁵D. G. Tempel, T. J. Martínez, and N. T. Maitra, *J. Chem. Theory Comput.* **5**, 770 (2009).
- ⁴⁶P. Elliott, J. I. Fuks, A. Rubio, and N. T. Maitra, *Phys. Rev. Lett.* **109**, 266404 (2012).
- ⁴⁷J. I. Fuks, P. Elliott, A. Rubio, and N. T. Maitra, *J. Phys. Chem. Lett.* **4**, 735 (2013).
- ⁴⁸M. Hellgren, D. R. Rohr, and E. Gross, *The Journal of chemical physics* **136**, 034106 (2012).